CONFIDENTIAL

NACA

RESEARCH MEMORANDUM

A STUDY OF THE FLOW FIELD BEHIND THE TRIANGULAR HORIZONTAL TAIL OF A CANARD AIRPLANE AT APPROXIMATELY THE VERTICAL-TAIL LOCATION BY MEANS OF A TUFT GRID

By Joseph L. Johnson, Jr.

Langley Aeronautical Laboratory
Langley Field, Va.

NATIONAL ADVISORY COMMITTEE
FOR AERONAUTICS

WASHINGTON

October 10, 1952

CONFIDENTIAL

NATIONAL ADVISORY COMMITTEE FOR AERONAUTICS

RESEARCH MEMORANDUM

A STUDY OF THE FLOW FIELD BEHIND THE TRIANGULAR HORIZONTAL TAIL OF A CANARD AIRPLANE AT APPROXIMATELY THE VERTICAL-TAIL LOCATION BY MEANS OF A TUFT-GRID

By Joseph L. Johnson, Jr.

SUMMARY

An investigation has been made in the Langley stability tunnel to study the flow field behind the triangular horizontal tail of a canard model by means of a tuft grid. The tuft grid was placed at approximately the vertical-tail location, which was about 6.0 horizontal-tail root chords behind the horizontal tail. This investigation was made in an effort to explain the results of previously reported investigations which showed that at high angles of attack canard models had positive static directional stability and negative damping in yaw with vertical tails off, and that the addition of a vertical tail at the rear of the fuselage gave a destabilizing increment to directional stability and a large stabilizing increment to damping in yaw. The tuft-grid studies showed that the trailing vortices from the horizontal tail produced a sidewash field over the model which probably accounted for these variations in stability.

INTRODUCTION

Several investigations have been made recently to determine the static stability and damping-in-yaw characteristics of canard models (refs. 1 to 3). These investigations showed that, at high angles of attack and high angles of incidence of the horizontal tail, the canard models tested had positive static directional stability with vertical tails off, apparently because of a sidewash which effectively reversed the angle of sideslip over the fuselage. This sidewash also caused the directional stability contributed by a vertical tail at the rear of the fuselage to be reduced. One of these investigations (ref. 3) showed

that in yawing flow a sidewash similar to that found in static tests caused a canard model to have negative damping in yaw with vertical tails off and caused the damping-in-yaw contribution of a vertical tail at the rear of the fuselage to be increased.

In an effort to obtain a better understanding of this sidewash and its effect on the static directional stability and control characteristics, some visual studies were made by attaching streamers of string to the fuselage and recording their action with a camera (ref. 3). The results obtained by this method were inadequate for determining the over-all characteristics of the flow field because only the direction of flow over the fuselage surface was shown. A technique for studying the complete flow fields associated with various model configurations has recently been developed at the Langley stability tunnel (ref. 4). This technique, known as the tuft-grid method, has proved to be very beneficial as an aid in explaining the stability characteristics of airplanes. It was decided, therefore, to make a study of the flow field behind a canard model by means of this tuft-grid method in an attempt to explain more completely the unusual static directional stability and damping characteristics noted in previous investigations of canard models.

In this investigation the model consisted of a fuselage with a high fineness ratio having a triangular canard horizontal tail with 63.5° sweep of the leading edge. The flow field behind the model, as shown on the tuft grid, was recorded as the angle of attack was varied from 0° to 20° with the model at -5° sideslip and as the angle of sideslip was varied from 0° to -5° with the model at an angle of attack of 20°.

SYMBOLS AND COEFFICIENTS

All forces and moments are referred to the stability system of axes originating at the center of gravity of the model. (See figs. 1 and 2.)

S	wing area, sq ft
b	wing span, ft
c	mean aerodynamic chord, ft
ρ	density of air, slugs/cu ft
α	angle of attack of fuselage center line, deg
i_t	angle of incidence of horizontal tail, positive with leading edge up, deg

V	airspeed, fps
q	dynamic pressure, $\frac{1}{2}\rho V^2$, lb/sq ft
β	angle of sideslip, deg
$\dot{\beta}$	angular velocity of sideslip, radians/sec
r	yawing angular velocity, radians/sec
C_L	lift coefficient, Lift/qS
C_Y	lateral-force coefficient, Lateral force/qS
C_n	yawing-moment coefficient, Yawing-moment/qSb

$$C_{n_\beta} = \frac{\partial C_n}{\partial \beta}$$

$$C_{n_{\dot{\beta}}} = \frac{\partial C_n}{\partial \frac{\dot{\beta} b}{2V}}$$

$$C_{n_r} = \frac{\partial C_n}{\partial \frac{rb}{2V}}$$

$$C_{Y_\beta} = \frac{\partial C_Y}{\partial \beta}$$

$$C_{l_\beta} = \frac{\partial C_l}{\partial \beta}$$

Model designations:

F	fuselage
W	wing
V	vertical tail
H	horizontal tail

APPARATUS AND MODEL

The tuft-grid survey was made in the Langley stability tunnel with the model mounted on a strut directly in front of a tuft grid. (See fig. 3 and ref. 4.) The survey apparatus consisted of a grid of wires with streamers of string 3 inches long attached at each intersection. This tuft grid was in a plane perpendicular to the direction of the free-stream velocity and was large enough to cover the part of the free-stream area affected by the model. A camera mounted downstream was used to record the action of the tufts during the tests. It should be pointed out that for illustrative purposes the model and tuft-grid assembly are shown much farther apart in figure 3 than was actually the case. In the tests, the tuft grid was placed at approximately the vertical-tail location which was about 6.0 horizontal-tail root chords behind the horizontal tail.

The model used in this investigation was the same model used in reference 2 with the wing removed and was similar to the model of reference 5. The horizontal tail was of triangular plan form with 63.5° sweep of the leading edge and had a $\frac{1}{4}$-inch flat-plate airfoil section with rounded leading edge. The fuselage was of circular cross section and had a fineness ratio of 12.90. For reference purposes a vertical rod was placed on the fuselage at the vertical-tail position. A three-view drawing of the model is shown in figure 2 and dimensional characteristics are given in table I.

TESTS

The tuft-grid survey was made at a dynamic pressure of 8.0 pounds per square foot, which corresponds to an airspeed of approximately 56.0 miles per hour at standard sea-level conditions and to a Reynolds number of 0.446×10^6 based on the mean aerodynamic chord of the wing shown in dashed outline in figure 2. (See table I.)

The tuft grid was used to study the flow field behind the model for a range of angle of attack from 0° to 20° while the model was at an angle of sideslip of -5° and, also, for a range of angle of sideslip from 0° to -5° while the model was at an angle of attack of 20°. All tests were made with the horizontal tail at an angle of incidence of 15°.

Included in the present report, with the results of the tuft-grid survey, are results of force and damping tests. Force tests of the model of the present investigation were made in the Langley free-flight

tunnel at a dynamic pressure of 3.0 pounds per square foot, which corresponds to a velocity of approximately 34.2 miles per hour and to a Reynolds number of 0.27×10^6 based on the mean aerodynamic chord of the wing of 0.85 foot. For comparative purposes, force and damping test data for another model of somewhat different geometric characteristics were taken from reference 3.

RESULTS AND DISCUSSION

Before the tuft-grid results are discussed, a brief review of the unusual static directional stability and damping-in-yaw characteristics noted for several canard airplane models in previous investigations is in order. The results of the tuft-grid survey will then be discussed and used to explain the static directional stability and damping-in-yaw characteristics.

Static Directional Stability and Damping-in-Yaw Characteristics

The static directional stability parameter C_{n_β} is presented for the model of the present investigation in figure 4. For completeness, the lateral stability parameters C_{Y_β} and C_{l_β} for this model are also presented in figure 4, but the discussion and correlation with tuft-grid results will be concerned only with C_{n_β}. The directional stability and damping-in-yaw parameters for the model of reference 3 are presented in figure 5.

The data of figure 4 show that the fuselage of the model was directionally unstable $\left(-C_{n_\beta}\right)$ over the angle-of-attack range. With the horizontal tail placed on the fuselage and deflected to an angle of incidence of 15°, the model was directionally unstable at low angles of attack but became stable $\left(C_{n_\beta}\right)$ at approximately 11° angle of attack and showed an increase in stability with increasing angle of attack. A vertical tail placed at the rear of the fuselage contributed a stabilizing increment to C_{n_β} over the angle-of-attack range. When the vertical tail was added to the fuselage—horizontal-tail combination, the contribution of the vertical tail to C_{n_β} was stabilizing at low angles of attack, but this increment decreased with increasing angle of attack and became negative in the higher angle-of-attack range. A comparison of the data

of figure 4 with data of reference 2 indicates that this increment of directional stability contributed by the vertical tail was somewhat different for the wing-on and wing-off configurations. The variation of this increment with angle of attack was similar for the two configurations, but the presence of the wing caused the vertical tail to become destabilizing at a lower angle of attack.

The results of figure 5 show that the canard model of reference 3 had generally the same static stability characteristics as the model of the present investigation: that is, an increase in C_{n_β} with increasing angle of attack for the tail-off configuration and a destabilizing increment to C_{n_β} contributed by a vertical tail located at the rear of the fuselage (at least at the angle of attack of 20° for which the model was tested). Tip tails located out of the sidewash field contributed an approximately constant increment of directional stability over the angle-of-attack range.

The damping-in-yaw $\left(-C_{n_r} + C_{n_{\dot\beta}}\right)$ data of figure 5 show a decrease in damping as the angle of attack increased for the configuration with all tails off and the configuration with tip tails on. The addition of the center tail to the model, however, gave a large stabilizing increment $\left(-C_{n_r} + C_{n_{\dot\beta}}\right)$ to the damping in yaw at 20° angle of attack.

Results of Tuft-Grid Survey

The general concept of the flow characteristics behind a lifting wing will be considered briefly before a discussion of the tuft-grid results. The difference in the flow on the upper and lower surfaces of a lifting wing causes a vortex motion in the boundary layers along the surfaces of the airfoil and in the wake behind it. The wake behind the wing is composed in part of a sheet of trailing vortices, and this sheet, as a result of the motions these vortices impart on each other, usually rolls up into two vortices. Results of references 6 and 7 show that the extent to which the vortices are rolled up depends upon the distance behind the wing and upon the lift coefficient, span loading, and aspect ratio of the wing. For wings with a low aspect ratio, the vortex sheet may become essentially rolled up into two trailing vortex cores within a chord or less of the trailing edge. For the canard design, the distance in chords between the horizontal-tail and vertical-tail location may be so great as to allow the vortex sheet from the horizontal tail to become essentially rolled up at the vertical-tail location. With tail incidences other than 15°, the flow pattern at the vertical-tail position would undoubtedly be somewhat different at a given angle of attack. Since the data of reference 2 indicate that similar effects on the static directional stability were obtained with horizontal-tail incidences other

than 15°, however, the results of the tuft-grid studies are probably generally representative of results that would be obtained with any horizontal-tail incidence.

The trailing vortices from the horizontal tail and the resulting flow field around the vortex cores for the canard model are visible in the tuft-grid results of figure 6. Since the view is from the rear of the model looking forward, the flow in the right vortex is in a counterclockwise direction and the flow in the left vortex is in a clockwise direction. The position of the right vortex with respect to the horizontal tail remains essentially unchanged as the angle of attack is increased, and this vortex appears to have no direct effect on the flow at the vertical-tail location. On the other hand, the left vortex does move with respect to the horizontal tail as the angle of attack is increased and it is this vortex which appears to be directly responsible for the sidewash over the vertical tail. At angles of attack of 4° and 8°, the vertical rod denoting the vertical-tail location is partly in the sidewash field above the left vortex. The sidewash is to the right and in a direction to increase the directional stability contributed by the tail as shown in figure 4. On the other hand, at angles of attack from 12° to 20°, the vertical-tail location is mostly in the flow field below the left vortex. This flow is predominantly to the left and in a direction to decrease the directional stability contributed by the vertical tail.

In analyzing the results of figure 6, it should be kept in mind that the tuft grid does not give a direct indication of the angle of sideslip at the vertical tail. The effective angle of sideslip at the tail is equal to the difference between the angle of sidewash measured by the tuft grid and the angle of sideslip of the model. When these two angles are equal and opposite, so that the effective angle of sideslip is zero, the contribution of the vertical tail to directional stability is zero. (The data of fig. 4 indicate that this condition occurs at an angle of attack of about 15°.) At higher angles of attack, the angle of sidewash indicated by the tufts is greater than the angle of sideslip of the model, so there is a reversal in the effective angle of sideslip at the tail. This reduction in effective angle of sideslip at low angles of attack and reversal at high angles of attack accounts for the decreasing directional-stability contribution of the vertical tail with increasing angle of attack. (See fig. 4.)

The tuft-grid results of figure 6 do not give a direct indication of the flow over the fuselage of the model since the tuft grid was located behind the fuselage for all tests. It appears from an analysis of the results of figure 6, however, that at high angles of attack the lower part of the vortex from the left tip of the horizontal tail flows over the fuselage to produce a resultant flow from right to left. This

analysis is substantiated by the flow-survey results of reference 2. In these flow surveys, in which tufts were attached to the upper surface of the fuselage, it was found that the flow across the fuselage at high angles of attack was in the opposite direction to that at low angles of attack. This effect of the horizontal tail on the flow over the fuselage accounts for the increase in the directional stability of the model with vertical tail off as the angle of attack is increased.

Results of tests made to show the effect on the flow field of changing the angle of sideslip while the angle of attack was held constant at 20° are shown in figure 7. At 0° angle of sideslip the two trailing vortices are symmetrically located with respect to the model. The flow fields around the cores of the vortices are of the same strength and of opposite directions so that the fuselage and vertical-tail location are in almost pure downwash. As the angle of sideslip is increased to -2.5°, the core of the left vortex moves downward and to the right while the core of the right vortex remains in about the same position relative to the horizontal tail. An increase in the angle of sideslip to -5° causes the left vortex to move farther downward and to the right with respect to the horizontal tail, and the fuselage and vertical-tail position move well into the sidewash field below the left vortex. This condition is the same as that shown for 20° angle of attack in figure 6. The trend of the change in the relative location of the vertical tail with respect to the sidewash field as the angle of sideslip is increased indicates that, at higher angles of sideslip (of the order of 10°), the vertical tail and the rearward part of the fuselage would be out of the sidewash field.

No oscillation tests were made in the present investigation, but the results of the flow surveys of reference 3 and the tuft-grid studies of reference 4 can be used to obtain an explanation for the negative damping of the fuselage at high angles of attack and the very large increment to damping in yaw produced by the addition of the center vertical tail, shown in figure 5. The results of the flow surveys of reference 3 indicated that in a yawing motion the canard model tested had a reversal in the direction of flow behind the horizontal tail which caused a sidewash over the fuselage and center vertical tail, similar to that found in static tests. In the tuft-grid studies (ref. 4) of the flow pattern behind a triangular wing oscillating in yaw, it was found that, as the wing oscillated, the vortex from the leading wing tip moved inboard while the vortex from the trailing wing tip remained relatively fixed with respect to the wing. As the model was oscillated the trailing vortices produced sidewash fields similar to those shown in figures 6 and 7. The tuft-grid surveys of reference 4 also showed that the motion of the trailing vortices and the resulting sidewash fields lagged behind the motions of the model. The resulting lag of sidewash could be another factor responsible for the large increase in damping in yaw produced by the addition of the center vertical tail.

SUMMARY OF RESULTS

An investigation was made in the Langley stability tunnel to study the flow field behind the horizontal triangular tail of a canard model by means of a tuft grid which was placed at approximately the vertical-tail location (about 6.0 horizontal-tail root chords behind the horizontal tail). The tuft-grid studies indicated that trailing vortices from the horizontal tail produced a sidewash field over the model which probably accounted for the fact that the model had positive static directional stability and negative damping in yaw at high angles of attack with vertical tails off and that the addition of a vertical tail at the rear of the fuselage gave a destabilizing increment to directional stability and a large stabilizing increment to damping in yaw.

Langley Aeronautical Laboratory,
National Advisory Committee for Aeronautics,
Langley Field, Va.

REFERENCES

1. Bates, William R.: Low-Speed Static Lateral Stability Characteristics of a Canard Model Having a 60° Triangular Wing and Horizontal Tail. NACA RM L9J12, 1949.

2. Draper, John W.: Low-Speed Static Stability Characteristics of a Canard Model With a 45° Sweptback Wing and a 60° Triangular Horizontal Control Surface. NACA RM L50G11, 1950.

3. Johnson, Joseph L.: Damping in Yaw and Static Directional Stability of a Canard Airplane Model and of Several Models Having Fuselages of Relatively Flat Cross Section. NACA RM L50H30a, 1950.

4. Bird, John D., and Riley, Donald R.: Some Experiments on Visualization of Flow Fields Behind Low-Aspect-Ratio Wings by Means of a Tuft Grid. NACA TN 2674, 1952.

5. Kraft, Christopher C., Jr., and Mathews, Charles W.: Determination by the Free-Fall Method of the Drag and Longitudinal Stability and Control Characteristics of a Canard Model at Transonic Speeds. NACA RM L50D04, 1950.

6. Spreiter, John R., and Sacks, Alvin H.: The Rolling Up of the Trailing Vortex Sheet and Its Effect on the Downwash Behind Wings. Jour. Aero. Sci., vol. 18, no. 1, Jan. 1951, pp. 21-32, 72.

7. Spreiter, John R.: Downwash and Sidewash Fields Behind Cruciform Wings. NACA RM A51L17, 1952.

TABLE I.- DIMENSIONAL CHARACTERISTICS OF THE CANARD MODEL USED IN THE INVESTIGATION

Fuselage:	
Length, in.	77
Fineness ratio	12.9
Cross section	Circular
Maximum diameter, in.	6
Horizontal tail:	
Airfoil section	Flat plate
Root chord, in.	12.0
Span, in.	12.0
Area (including area covered by fuselage), sq ft	0.50
Mean aerodynamic chord, in.	6.0
Aspect ratio	2.0
Sweepback, deg	63.5
Dihedral, deg	0
Tail length (from L.E. of M.A.C. of wing to L.E. of M.A.C. of tail), in.	47.25
Wing (static data based on wing of ref. 2):	
Airfoil section	NACA 65-009
Chord (normal to L.E.), in.	7.20
Span, in.	42.00
Area, (including area covered by fuselage), sq ft	2.95
Mean aerodynamic chord, in.	10.20
Aspect ratio	4.1
Sweepback (0.50c), deg	45.0
Taper ratio	1.0
Incidence, deg	0
Dihedral, deg	0
Twist, deg	0
Vertical tail (Used on model for static tests. See ref. 2.):	
Airfoil section	NACA 65-009
Chord (normal to leading edge), in.	5.05
Span, in.	10.70
Area (to fuselage center line), sq ft	0.53
Aspect ratio	1.5
Sweepback (0.50c), deg	45.0
Taper ratio	1.0
Tail length (from L.E. of M.A.C. of wing to L.E. of M.A.C. of tail), in.	20.57

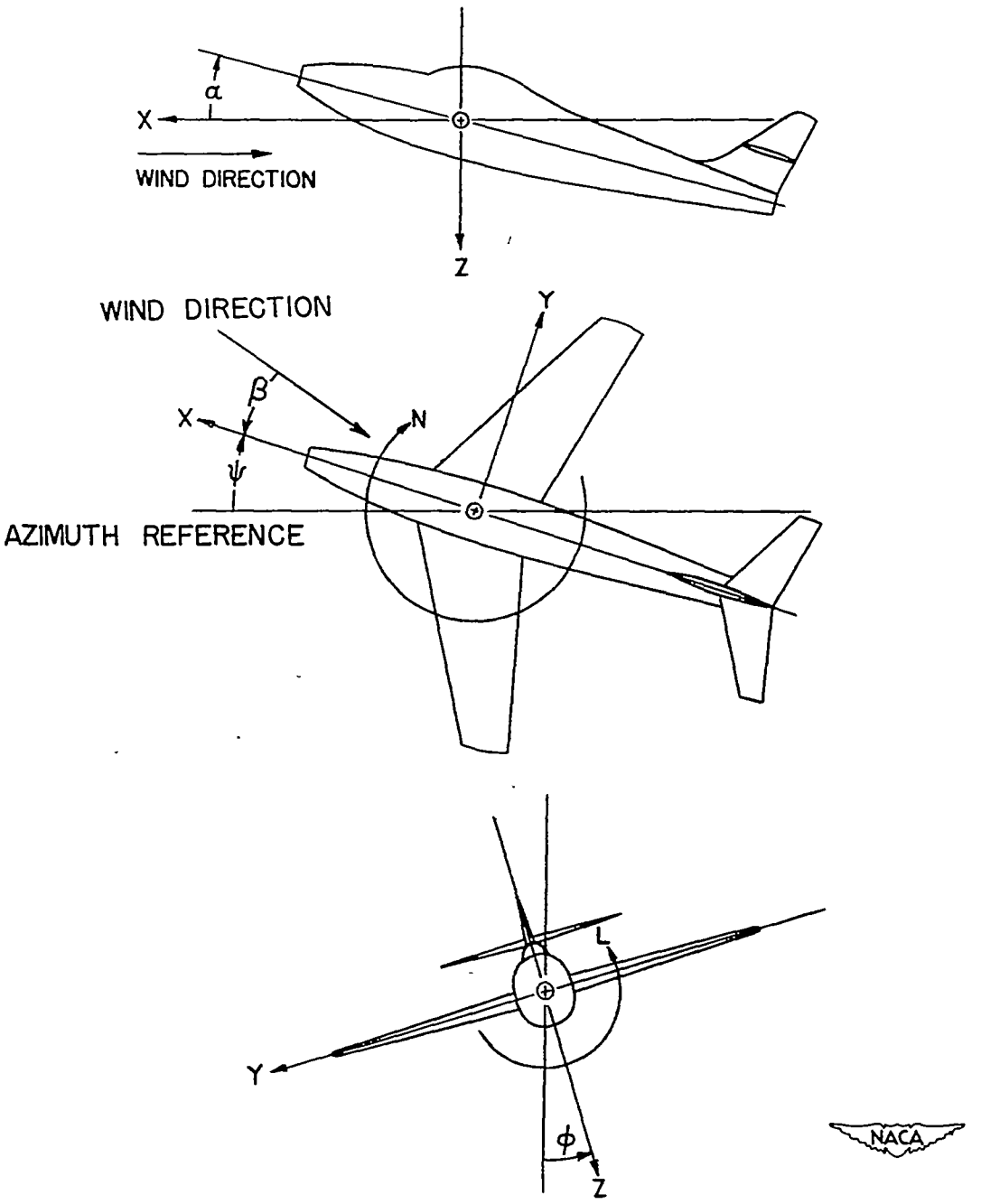

Figure 1.- The stability system of axes. Arrows indicate positive directions of moments, forces, and angles. This system of axes is defined as an orthogonal system having the origin at the center of gravity and in which the Z-axis is in the plane of symmetry and perpendicular to the relative wind, the X-axis is in the plane of symmetry and perpendicular to the Z-axis, and the Y-axis is perpendicular to the plane of symmetry. At a constant angle of attack, these axes are fixed in the airplane.

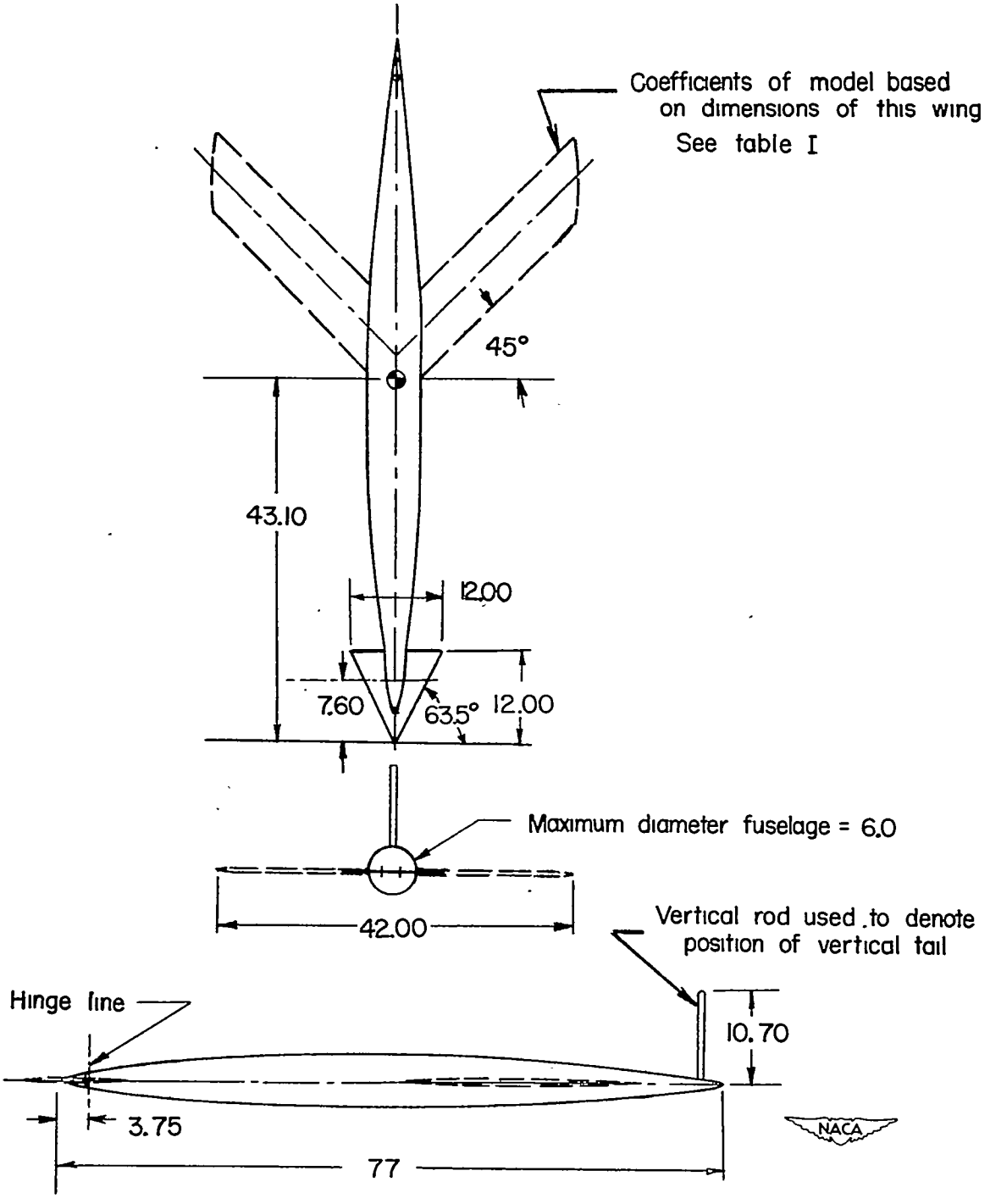

Figure 2.- Three-view drawing of model used in the investigation. All dimensions are in inches.

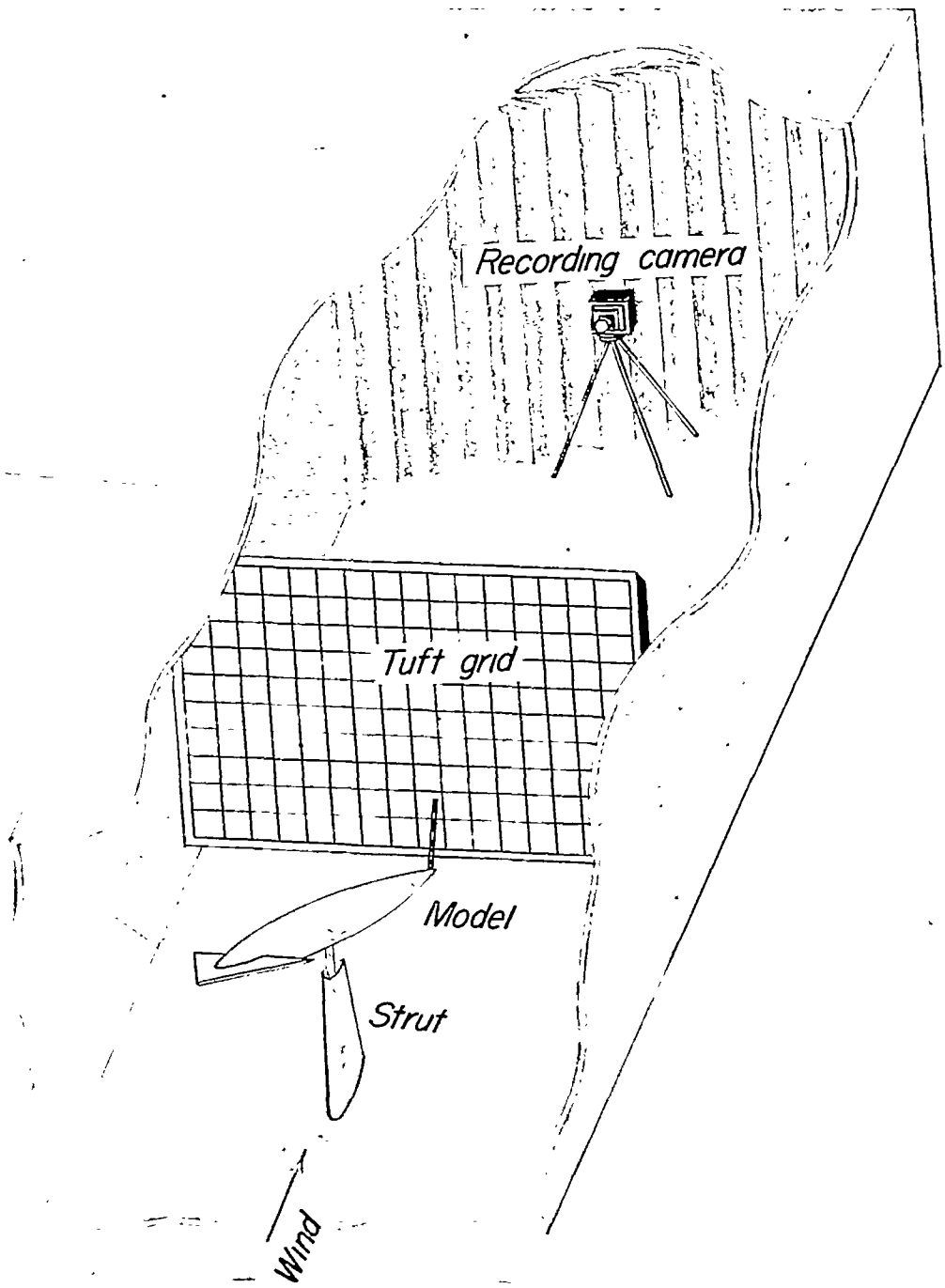

Figure 3.- General arrangement of tuft-grid apparatus in the Langley stability tunnel.

NACA

L-76141

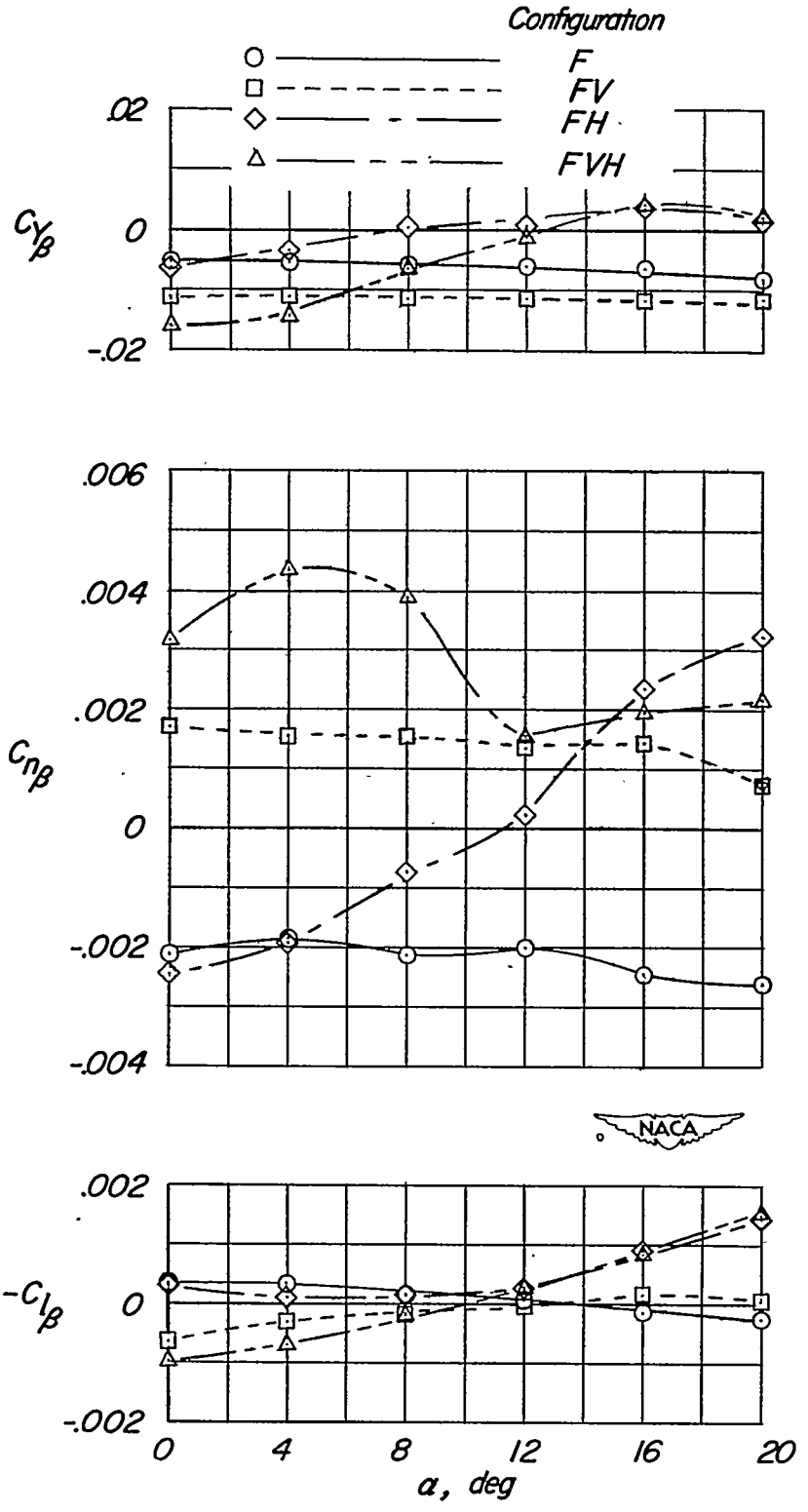

Figure 4.- Lateral stability characteristics of model used in the investigation. For FH and FVH configurations, $i_t = 15^\circ$.

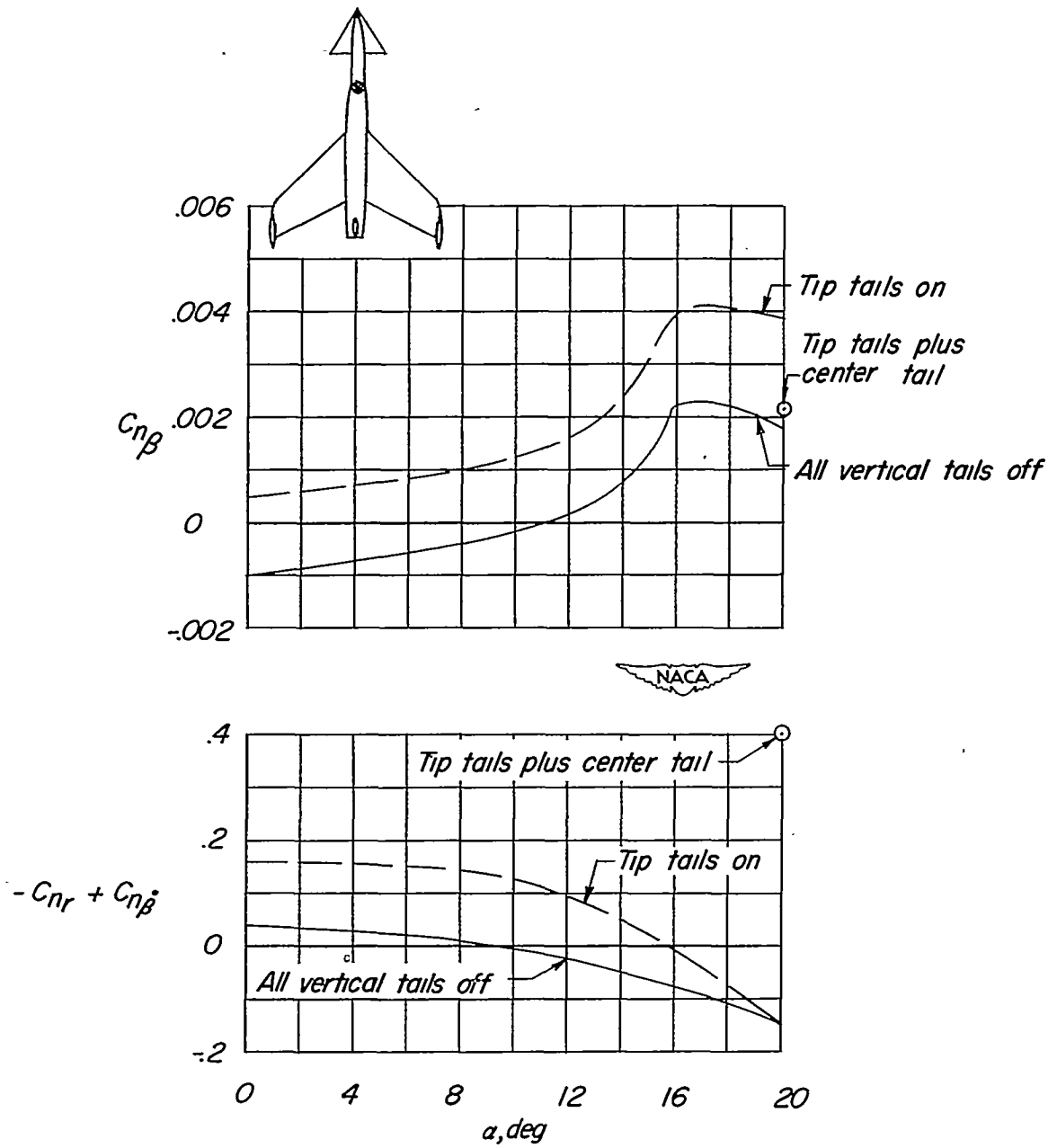

Figure 5.- Static directional stability and damping-in-yaw characteristics of the canard model of reference 3. $i_t = 15^\circ$.

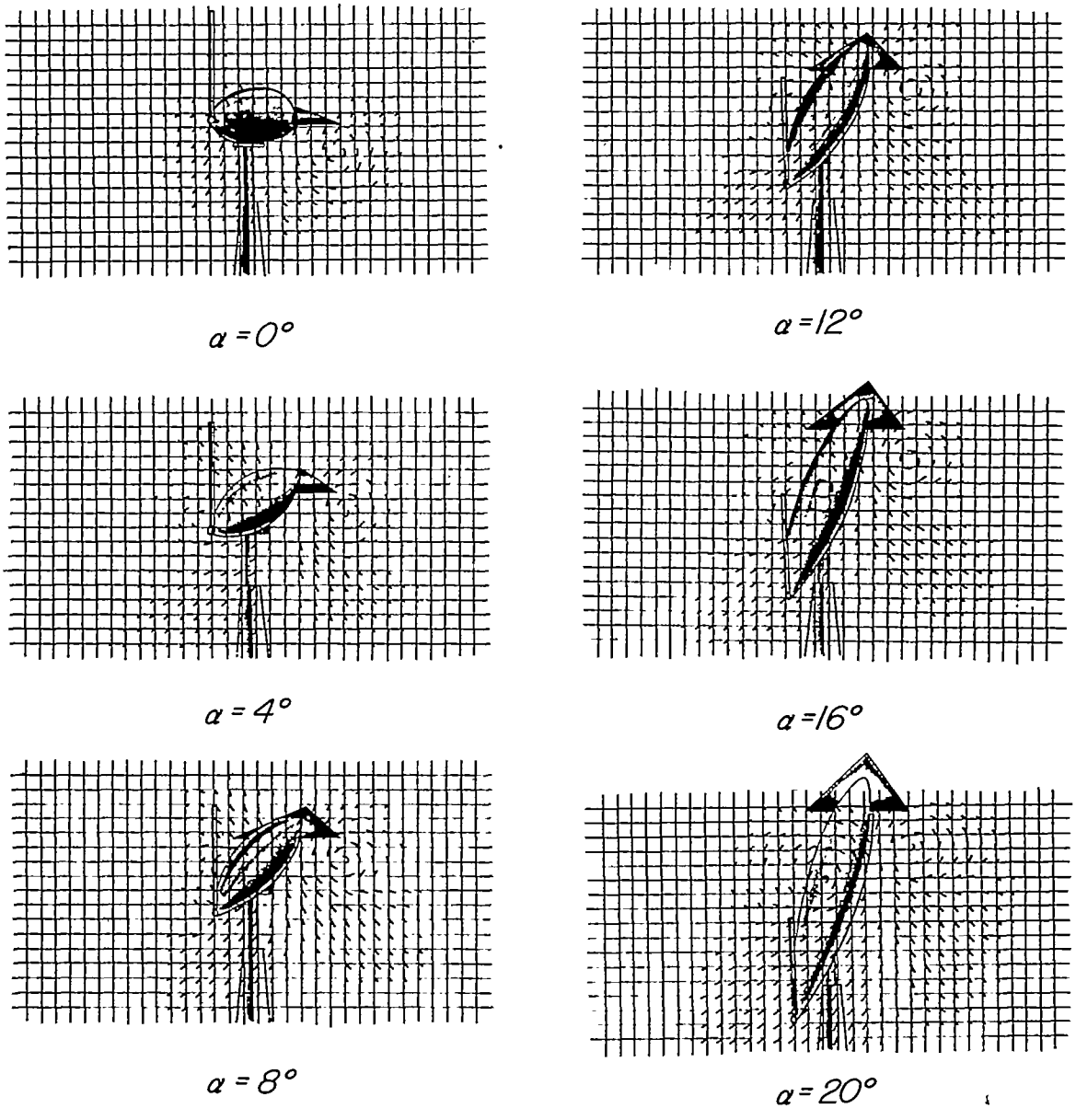

Figure 6.- Effect of angle of attack on the flow pattern behind the canard model used in the investigation. Configuration FH. $\beta = -5^{\circ}$; $i_t = 15^{\circ}$.

NACA

L-76140

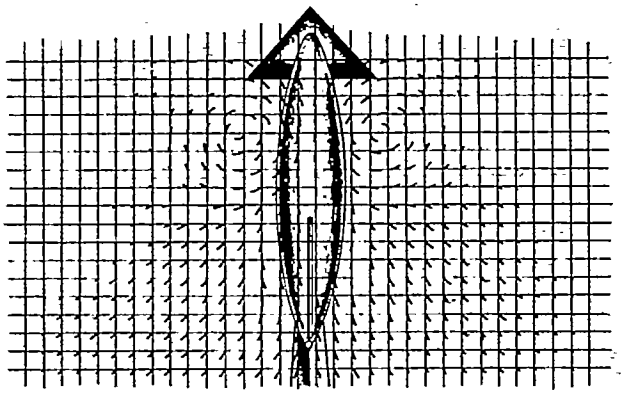

$\beta = 0°$

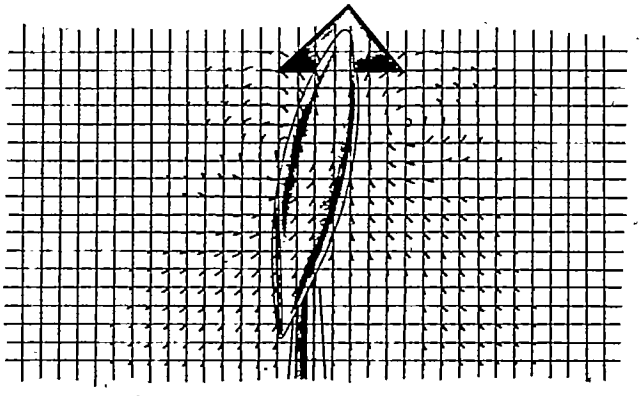

$\beta = -2.5°$

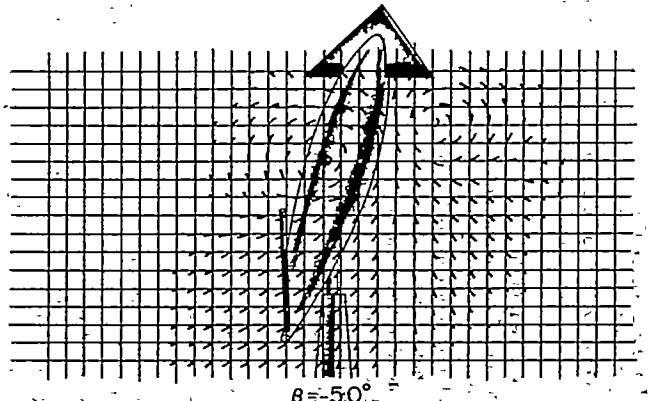

$\beta = -5.0°$

Figure 7.- Effect of angle of sideslip on the flow pattern behind the canard model used in the investigation. Configuration FH. $\alpha = 20°$; $i_t = 15°$.

NACA

L-76139